Asia-Pacific Journal of Chemical Engineering

WILEY | Curtin University

RESEARCH ARTICLE

Exploring Thermal Dynamics of Periodic Bar Motion on Natural Convection in a Square Cavity

Nehila Tarek[1] | Muneer Ismael[2,3] | Benachour Elhadj[1] | Mikhail Sheremet[4] | Mohammad Ghalambaz[5,6]

[1]ENERGARID Laboratory, Tahri Mohamed University of Bechar, Tahri Mohamed University of Bechar, Bechar, Algeria | [2]Mechanical Engineering Department, Engineering College, University of Basrah, Basra, Iraq | [3]College of Engineering, University of Warith Al-Anbiyaa, Karbala, Iraq | [4]Laboratory on Convective Heat and Mass Transfer, Tomsk State University, Tomsk, Russia | [5]Department of Mathematical Sciences, Saveetha School of Engineering, SIMATS, Chennai, India | [6]Refrigeration and Air conditioning Technical Engineering Department, College of Technical Engineering, The Islamic University, Najaf, Iraq

Correspondence: Nehila Tarek (nehila.tarek@univ-bechar.dz)

Received: 11 August 2025 | **Revised:** 3 September 2025 | **Accepted:** 10 September 2025

Funding: The authors received no specific funding for this work.

Keywords: moving mesh | natural convection | moving bar | periodic movement | square cavity

ABSTRACT

Understanding the effects of fixed and moving bars allows for the design of more efficient thermal systems by using dynamic obstacles to optimize natural convection. This study complements several numerical studies on the effect of bars in a closed cavity. We examine the phenomenon of heat transfer by natural convection within a square cavity heated on the left side and cooled on the right side, with an adiabatic bar undergoing periodic vertical motion with an amplitude U_{bar} and period T_{bar}. We use the finite element method to solve the guiding dimensionless nonlinear equations. Our focus is on the effect of the bar movement direction, displacement amplitude U_{bar} (0.1–0.4), displacement period T_{bar} (1/3–1), bar width B (0.05–0.2), Rayleigh number Ra (10^4–10^7), and number of bars N (1–3) on the average Nusselt number, streamlines, and isotherms distribution. The results show that increasing Ra significantly improves heat transfer. Maximum heat transfer occurs at $U_{bar}=0.1$ and $T_{bar}=1$. Increasing bar width and number negatively affects the average Nusselt number. This work contributes to understanding how dynamic obstacles can optimize natural convection, offering insights for the design of more efficient thermal systems.

1 | Introduction

The study of energy transfer by convection is of great interest to researchers and institutions due to its involvement in numerous engineering and industrial applications. For example, in the electronics field (cooling of electronic components), energy sector (cooling of solar panels and batteries), buildings (design of buildings utilizing natural ventilation for cooling and air circulation) [1], and aerospace (heat management in satellites and spacecraft).

One of the proposed solutions to control and regulate energy transfer is the integration of objects with different shapes inside a fixed cavity. Following, we present the most significant recent studies on this topic and the key results obtained. The study of obstacles within cavities has been the subject of extensive scientific research.

A numerical study conducted by Raji et al. [2] examined the effect of blocks with different numbers ($N=1$, 4, 16, and 64) and thermal conductivity ratios (Kr) on heat transfer by natural convection. The findings revealed that an increase in the number of blocks and the thermal conductivity ratio can lead to a significant reduction in the Nusselt number. In another study by Boulahia [3], the researchers investigated heat transfer by mixed convection of nanofluids in a square cavity with three triangular

heating blocks. The results showed that there is an optimal position for the triangular heating blocks where the heat transfer rate is maximized. The impact of a rectangular heat source on the magnetohydrodynamic (MHD) hybrid convection flow in a lid-driven cavity was addressed by Umme et al. [4]. The results demonstrated that the average Nusselt number significantly decreased with increased magnetic field intensity and heat generation, but it increased with heat absorption. Another study explored convection flows combined with the presence of a square cylinder placed in the center of a square cavity. They concluded that a decrease in kinetic energy capacity is observed due to the creation of Lorentz forces. The lattice Boltzmann method (LBM) was used in [5] to simulate the convection phenomenon in a cavity for a water-TiO_2 nanofluid with a hot obstacle. The results showed that the dimensions of the obstacle can affect the Nusselt number: an increase in obstacle dimensions to 0.5 L increased the Nusselt number, but further increase to 0.7 L resulted in a decrease. A three-dimensional numerical study by Aich et al. [6] examined heat transfer within a cubic cavity filled with graphene-water nanofluids. Inside this cavity was a tree-shaped obstacle located at the bottom center and a horizontal magnetic field (MF). The results indicated that adding graphene significantly improved the thermal conductivity of the fluid, enhancing heat transfer. However, increasing the dimension (length) of the obstacle slightly negatively impacted heat transfer efficiency.

In a circular cavity with a variable number of obstacles, Mirzaei et al. [7] studied the MHD heat and mass transfer phenomena. The results indicated that heating the upper obstacles decreased the total Nusselt number, while heating the lower obstacles had the opposite effect. As the number of obstacles inside the cavity increased, heat transfer improved. A recent study by Elkhazen [8] addressed the impact of an adiabatic obstacle on flow and electrical charge during electrohydrodynamic (EHD) natural convection. The results showed that depending on the position and size of the obstacle, convective transfer could increase by 27% or decrease by 21%. The study presented five multiparametric correlations for determining the Nusselt number, intended for engineering applications.

The study by Nabwey et al. [9] examined unstable free convection flow of MHD in an inclined wavy cavity with a hybrid nanofluid (aluminum oxide/copper-water) and a square obstacle. They concluded that improving porosity and increasing the volume fraction of nanoparticles positively affected the average Nusselt number and heat transfer. For a phase change study by Yan et al. [10], natural convection of materials in a cavity was addressed, exploring the effect of an adiabatic obstacle and fin using the Boltzmann method. They found that modifying the dimensions of the adiabatic fins from Yf = 0.1 to Yf = 0.7 doubled the fusion time at approximately 80% fusion of the PCM. Another study by Rashid et al. [11] focused on the impacts of nanoparticle shape on nanofluid flow in a square cavity with a fixed circular obstacle at the cavity's center. They concluded that non-spherical nanoparticles (e.g., diamond-water) performed better in temperature distribution and heat transfer. Finally, natural convection in a cavity filled with nanofluid with obstacles of different shapes (circular, square, and diamond) under the influence of a uniform magnetic field and uniform heat generation was presented by Selimefendigil [12]. The key results showed that the average heat transfer decreased by 21.35%, 32.85%, and 34.64% for cavities with circular, diamond-shaped, and square obstacles, respectively, compared to the cavity without obstacles. A study conducted by Ahmad et al. [13] dealing with the effects of an isothermal source and sink on natural transfer and entropy generation for Casson fluids found that length and width are closely related to the rates of entropy, mass, and heat transfer. The phenomenon of double diffusion in a non-Newtonian fluid within an offset cavity is addressed by Majeed et al. [14]; the numerical results show that convective mass transfer is significantly correlated with the Lewis number. Thus, when the power index increases, convection also proves to be an increased means of heat and mass transmission. A study conducted by Shafee Ahmad et al. [15] examined the coupling of natural convection flow, entropy generation, as well as rigid structures (fins); the non-Newtonian working fluid and an inclined magnetic field is applied. The results show that the inclusion of fins results in greater resistance to fluid displacement, which leads to a decrease in the Nusselt and Sherwood numbers. The thermal and mechanical coupling of the flow of a suspension of iron (II, III) oxide (Fe_3O_4) microparticles in a coaxial cylindrical annular space under a magnetic field is examined by Si-Liang Sun et al. [16]. The results indicate that increasing the Reynolds and Hartmann numbers improves the heat transfer capacity of the Taylor vortex flow.

Unlike previous works that focused on stationary obstacles, this study investigates the effect of periodic obstacle motion on natural convection and its impact on heat transfer. The findings provide original insights into the role of dynamic obstacles, with potential applications in electronic cooling, micro/nanoscale systems, and compact energy devices. The vibration can be achieved through non-contact actuation methods (e.g., piezoelectric), ensuring minimal wear, and since the vibration Reynolds number remains much smaller than the Rayleigh number, the heat transfer process is still governed by natural convection.

2 | Mathematical Formulation

2.1 | Problem Definition and Assumptions

In this research, we are interested in the phenomena of natural convection within a square cavity of length L. We analyze the periodic vertical movement of a bar(s) with dimensionless length and width A and B located at the center of the cavity (coordinates X = 0.5 and Y = 0.5) and the working fluid air. The temperature of the right and left walls of the cavity is kept constant at Tc and Th, respectively, as shown in Figure 1.

The equations governing the phenomenon of natural convection can be presented in dimensional and non-dimensional forms [17]. In our investigation, we have ignored the heat dissipation and the variations of dependent variables in the direction normal to the X-Y plane. The thermophysical properties are considered constant except for the density, which varies with temperature based on the Boussinesq approximation. The flow of air is considered laminar, Newtonian, and incompressible. For the sake of brevity, only the non-dimensional form is presented in this study. The following non-dimensional parameters are adopted:

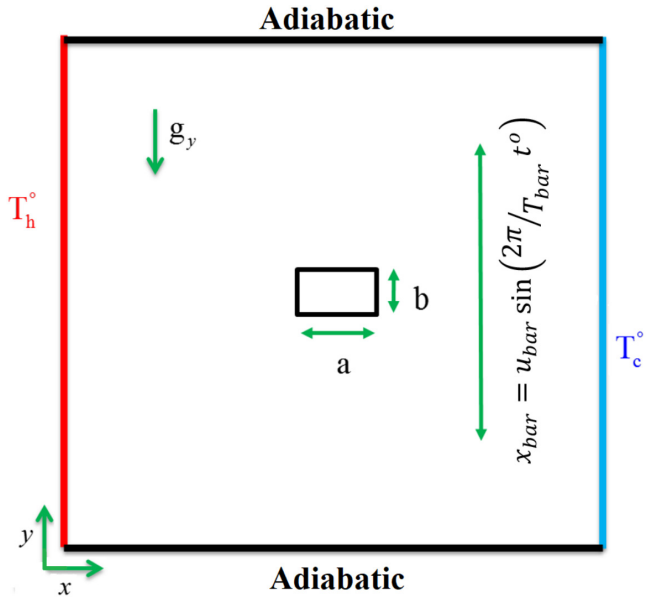

FIGURE 1 | A physical representation within a square enclosure with adiabatic bar and its corresponding system of coordinates.

$$(X_{bar}, X, Y, L, A, B) = \frac{(x_{bar}, x, y, a, b)}{L}\,(u_{air}, v_{air}) = \frac{(u^\circ_{air}, v^\circ_{air})L}{\alpha_{air}}\,t = \frac{t^\circ \alpha_{air}}{L^2},$$
$$T = \frac{(T^\circ - T^\circ_c)}{(T^\circ_h - T^\circ_c)}\,P = \frac{L^2 p^\circ}{\rho_{air}\alpha^2_{air}},\,\psi = \frac{\psi^\circ L^2}{\alpha_{air}} \tag{1}$$

The conservation of mass equation ensures that the flow field satisfies the principle of continuity.

$$\nabla \cdot u_{air} = 0 \tag{2}$$

The momentum equations describe the fluid motion under the influence of buoyancy and viscous forces inside the cavity [18]:

$$\frac{\partial u_{air}}{\partial t} + u_{air} \cdot \nabla u_{air} + \nabla P - Pr\nabla^2 u_{air} = PrRaT \tag{3}$$

The energy equation that governs the heat transfer due to both conduction and convection:

$$\frac{\partial T}{\partial t} + u_{air} \cdot \nabla T = \nabla^2 T \tag{4}$$

The non-dimensional parameters are defined as follows.

$Ra = \frac{g_y \beta (T_h - T_c) L^3}{\upsilon_{air}\alpha_{air}}$ (Rayleigh number) and $Pr = \frac{\upsilon_{air}}{\alpha_{air}}$ (Prandtl number).

The bar is followed by a periodic vertical displacement with amplitude U_{bar} and period T_{bar}; this displacement is represented by the following equation:

$$X_{bar} = U_{bar} sin\left(\frac{2\pi}{T_{bar}} t^\circ\right) \tag{5}$$

2.2 | Boundary Conditions

Considering the boundary conditions, the thermal and dynamic characteristics of the walls are expressed in dimensionless coordinates as follows:

- On the left wall: $T_h = 1$, and on the right wall $T_c = 0$
- The upper and lower horizontal walls as well as to the bar surface $u_{air} = v_{air} = 0$ and $\frac{\partial T}{\partial n} = 0$

The parameter of interest is the local and the average Nusselt numbers on the left wall to quantify the strength of the natural convection at any point over the hot wall. It can be evaluated as:

$$Nu = hL / k^{air} \tag{6a}$$

where h is the convective heat transfer coefficient, L is the characteristic length of the cavity, and K^{air} is the thermal conductivity of air.

The average Nusselt number is expressed as:

$$Nu_{local} = \frac{dT}{dn} \tag{6b}$$

$$\overline{Nu} = \int Nu_{local} d\tau \tag{6c}$$

The stream function is introduced as:

$$u_{air} = \frac{\partial \psi}{\partial y}, v_{air} = -\frac{\partial \psi}{\partial x} \tag{7}$$

3 | Numerical Simulation

In this study, the Galerkin finite element method with moving mesh is used for the numerical simulation of this problem. The fundamental nonlinear equations are described by the finite element method and solved numerically, with a detailed presentation of this method provided in [19, 20]. For the vertical movement of the bar, we used the moving mesh technique [21], with details on this type of mesh presented in [22, 23]. The solution to the moving mesh equations smoothly moves the mesh nodes on the surface and within the fluid mass. The Navier–Stokes equations are solved on a moving frame fully coupled to the mesh equations. The numerical calculation estimates an error of less than 10^{-6}.

3.1 | Mesh Testing

In this step, we present the mesh model used in this study (as shown in Figure 2). It is a moving mesh that illustrates the three different positions of bar A: at the base, B: at the center, and C: at the height of the cavity. It also shows the deformation appropriated by the mesh, where we used a quadratic mesh for the air. To ensure that the numerical results are independent of the mesh size, a mesh sensitivity test was performed for four different cases (A, B, C, and D), as presented in Table 1. For each case, the number of elements and mesh element domains is presented.

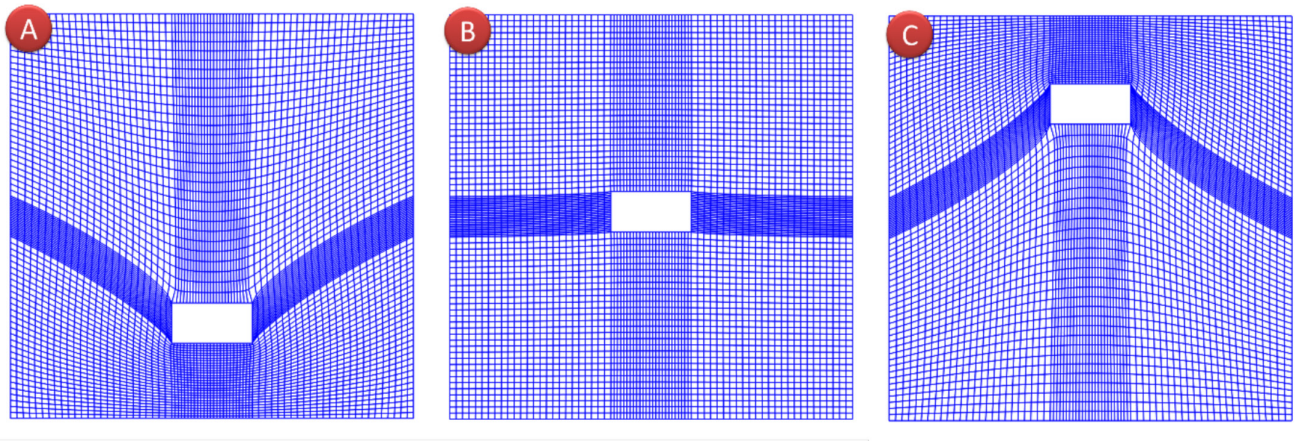

FIGURE 2 | The constructed mesh of the model under examination.

TABLE 1 | Sensitivity testing of the mesh involves examining various mesh sizes.

	Cases			
	Case A	**Case B**	**Case C**	**Case D**
Domain elements	2250	3800	**5750**	8100
Boundary elements	400	520	**640**	760

Figure 3 represents the variation of the average Nusselt number with respect to the mesh type for the parameters Ra = 1E5, $T_{bar} = 2/3$, $B = 0.1$. In the figure, we can observe that the curves are identical for a time interval between 0 and 0.2. The variation in the number of elements appears in the fluctuation peaks; as the number of elements in the domain increases from cases A to D, the curves become closer, with near-identical results between cases C and D. This indicates that the results have become independent of the number of elements.

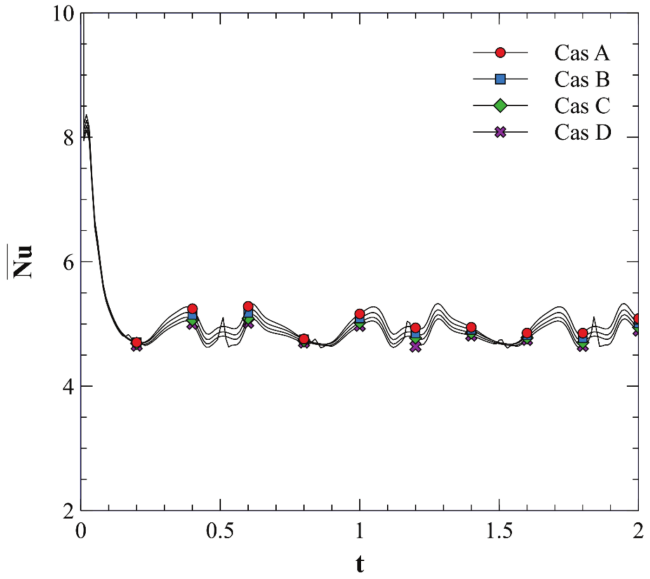

FIGURE 3 | Grid testing of $\overline{Nu}$ on the hot wall with different grid cases at $U_{bar} = 0.4$, Ra = 10^5, $T_{bar} = 2/3$, B = 0.1.

3.2 | Validation

We conducted a validation study by comparing our current numerical results with existing experimental and numerical data to demonstrate the reliability of the results presented in the following section.

Figures 4 and 5 present a numerical validation with the study of Kim et al. [24], where they numerically studied the phenomenon of natural convection induced by a temperature difference between a cold outer square enclosure and a hot inner circular cylinder. For different Rayleigh numbers varying over the range from 1E3 to 1E6. Figures 4 and 5 show the distribution of isotherms and streamlines results from Kim et al. [24] and the present results for a circular cylinder with dimension $R = 0.2$, at Ra = 1E6. A simple comparison of figures A and B reveals a good agreement between the two.

In a second validation (in Figure 6), we compared our results with a previous study on natural convection in a partially heated square cavity, conducted both numerically and experimentally. This validation was based on the local Nusselt number, a crucial parameter in our study. The results of the comparison are presented in the figure, with parameters fixed at Ra = 1.2×1E5 and a heat source length equal to 4/5. Our results fall within the expected range, confirming the robustness of our approach. Eventually, the benchmark work of Val Davis [26] is also verified by the present numerical solution. The results tabulated in Table 2 demonstrate a maximum percentage error of 0.18%, which indicates to a high level of reliability in the present numerical solution.

Finally, validation was carried out using the results of Raji et al. [27], where natural convection in a square cavity with horizontal walls subjected to different heating models was examined. The results of this comparison are presented in Figure 7, which shows the variation of the average Nusselt number over time for the following parameters: $a = 0.2$ (amplitude of the cold sinusoidal temperature), Ra = 10^5, and $\tau = 0.5$ (frequency of the sinusoidal cold temperature). The graphical results show good agreement, with an uncertainty of less than 2%.

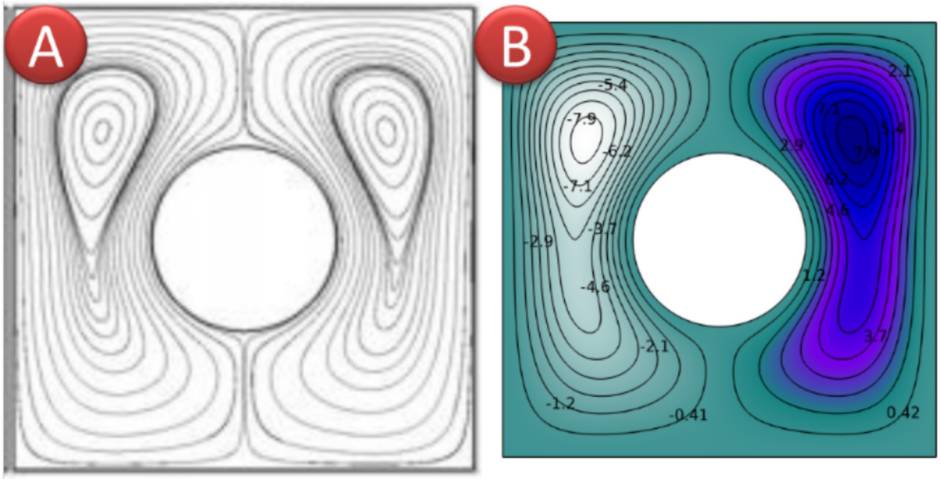

FIGURE 4 | Comparison of streamlines (A) numerical results of [24] and (B) the present numerical results for $Ra = 10^6$.

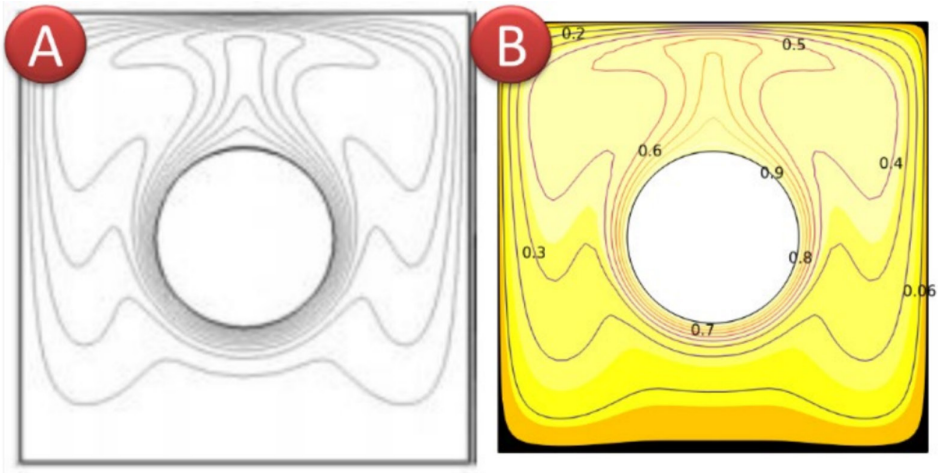

FIGURE 5 | Comparison between the isotherms, where (A) represents the numerical result from [24] and (B) denotes the present study for $Ra = 10^6$.

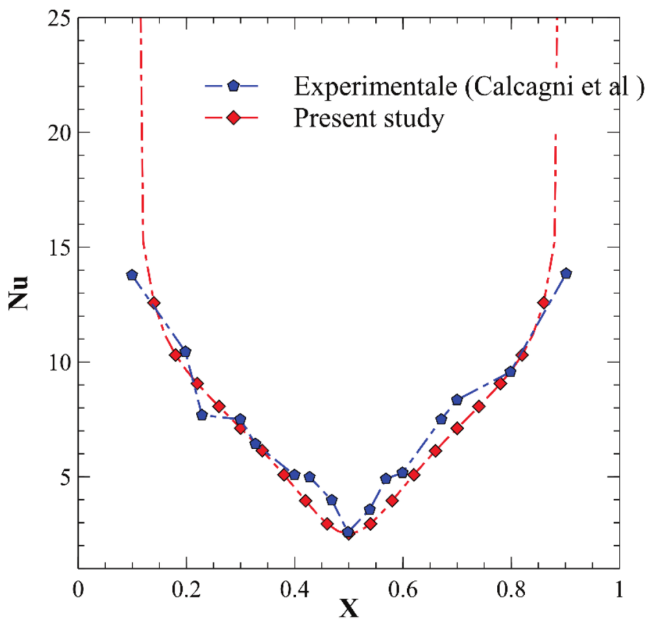

FIGURE 6 | The local Nusselt number comparison in the experimental work conducted by Calcagni et al. [25] and the current numerical study.

TABLE 2 | Comparison of $\overline{Nu}$ number validation results with literature results for three Rayleigh numbers of 1E4, 1E5, and 1E6.

	Ra		
	10^4	10^5	10^6
Val Davis [26]	2.2430	4.5190	8.8800
Present study	2.2441	4.5109	8.8453
Error	0.05%	0.18%	0.04%

4 | Results and Discussion

This part of the study focuses on the numerical results and discussions regarding the different parameters influencing the phenomenon of natural convection within the cavity with a moving adiabatic bar. The dimensionless parameters considered include the displacement period T_{bar} with values of 1/3, 2/3, and 1; the amplitude of displacement of the bar (U_{bar}) ranging from 0.1 to 0.4; and the direction of movement of the bar (horizontal and vertical). The width of the bar (B) varies from 0.05 to 0.2, and the Rayleigh number ranges from 1E4 to 1E7. Additionally,

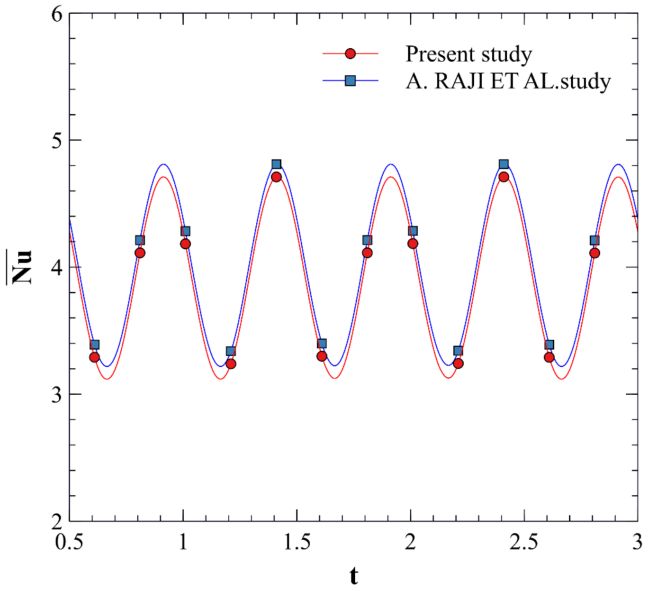

FIGURE 7 | The Nusselt number comparison in numerical work conducted by A. Radji et al. [27] and the current numerical study.

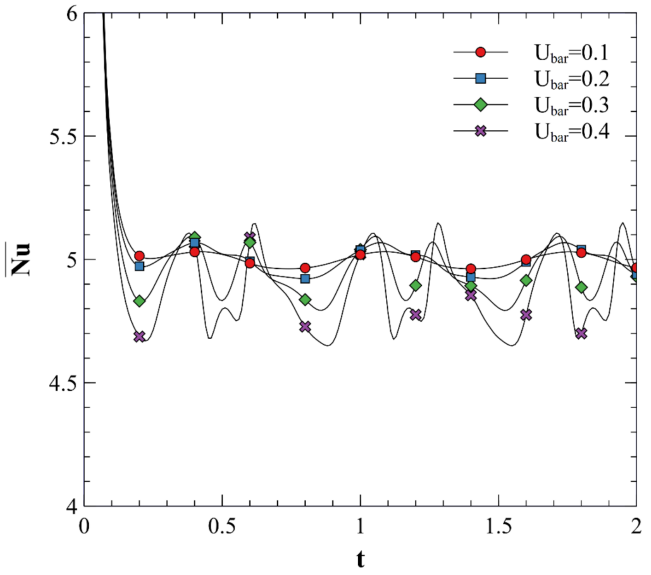

FIGURE 8 | The influence of the amplitude of displacement of the bar on $\overline{Nu}$ over time dimensionless at $Ra = 10^5$, $B = 0.1$, $T_{bar} = 2/3$.

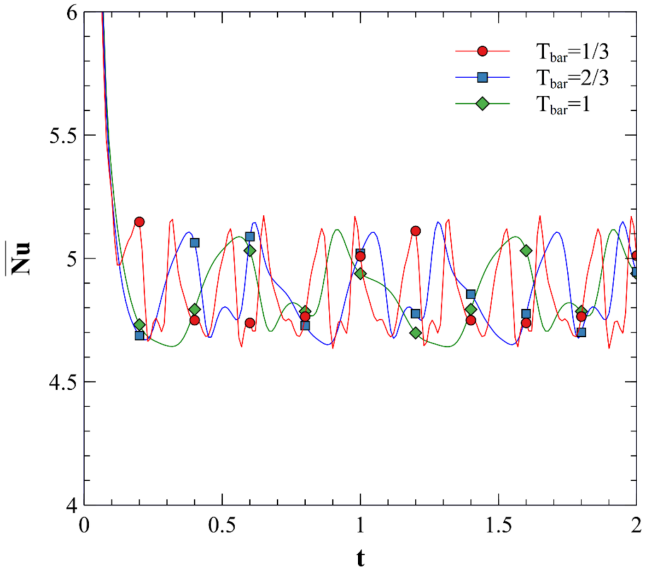

FIGURE 9 | The influence of the oscillation period on $\overline{Nu}$ over time dimensionless at $Ra = 10^5$, $U_{bar} = 0.4$, $B = 0.1$.

the study considers the number of bars ($N = 1, 2, 3$). The time interval considered is $0 < t < 2$, while maintaining Prandtl number ($Pr = 0.71$).

4.1 | Bar Movement Effect

Regarding the characteristics of the oscillating bar, we varied the following parameters to inspect its impact: the periodical movement, represented by the period T_{bar}; the extent of movement, represented by the amplitude U_{bar}; and the direction of movement, both horizontal and vertical. The influence of these parameters on the average Nusselt number is presented graphically in Figures 8, 9, and 10.

Figure 8 demonstrates the effect of the amplitude of displacement of the bar on the average Nusselt number for $Ra = 10^5$, $B = 0.1$, and $T_{bar} = 2/3$ over a dimensionless time interval between 0 and 2. Four values of U_{bar} are considered: 0.1, 0.2, 0.3, and 0.4, corresponding to displacements of 0.2, 0.4, 0.6, and 0.8, respectively (following a sinusoidal function).

At the initial stage ($t < 0.15$), the thermal field is dominated by conduction, which explains the similarity of the curves for different amplitudes. Once convection develops, the bar's motion induces periodic fluctuations in heat transfer. For small amplitudes ($U_{bar} = 0.1$), the disturbance is weak and mixing remains limited, while larger amplitudes (e.g., $U_{bar} = 0.4$) enhance fluid oscillations, leading to stronger but less stable convective transport.

The maximum Nusselt number corresponds to the position of the bar at the center of the cavity, while the minimum values correspond to the bar's positions at the top and base of the cavity. This suggests that the position of the bar during its movement can lead to either an improvement or a reduction in heat transfer. We also record the increase in the amplitude of movement causing a decrease of 1% in heat transfer each time U_{bar} increases by 0.1.

Figure 9 shows the effect of the period of movement of the bar on the average Nusselt number for $Ra = 10^5$, $B = 0.1$, and $U_{bar} = 0.4$ over a dimensionless time interval between 0 and 2. Three values of T_{bar} are considered: 1/3, 2/3, and 1. For short times, conduction dominates and the curves overlap, but as time progresses, the effect of oscillation period becomes evident. A longer period ($T_{bar} = 1$) allows the system to adjust smoothly, resulting in uniform fluctuations, while shorter periods ($T_{bar} = 1/3$) inject higher-frequency disturbances that destabilize the flow and reduce the regularity of heat transfer.

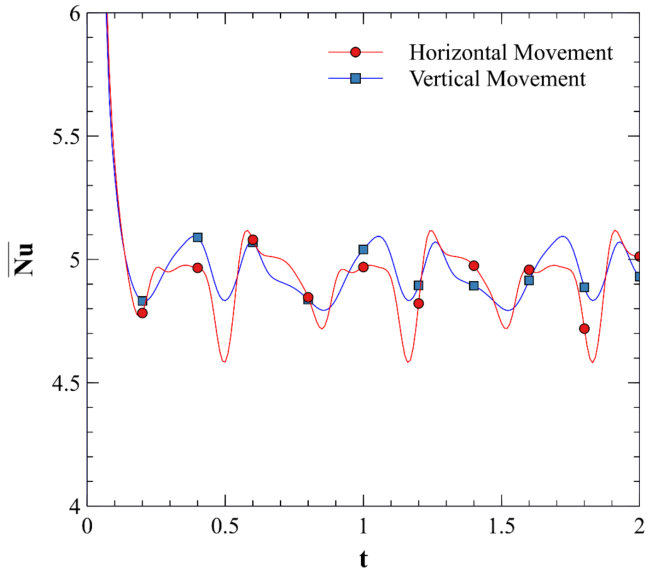

FIGURE 10 | The influence of the direction of movement of the bar on $\overline{Nu}$ over time dimensionless at Ra = 10^5, U_{bar} = 0.3, B = 0.1, and T_{bar} = 2/3.

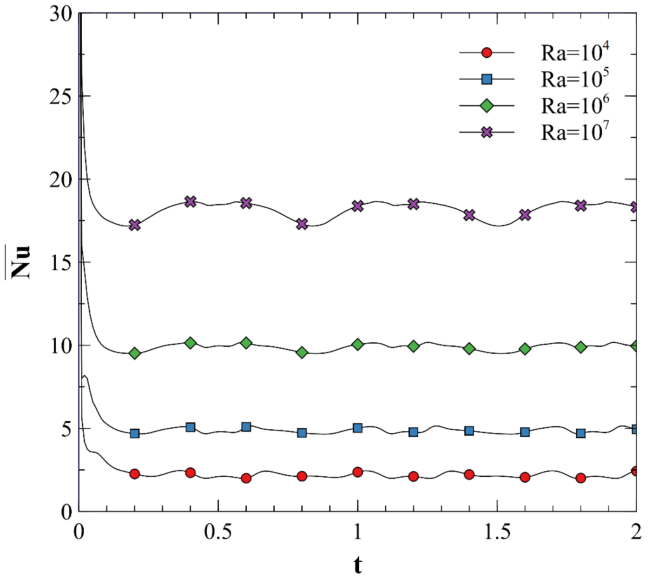

FIGURE 11 | The influence of the Rayleigh number on $\overline{Nu}$ number over time dimensionless at U_{bar} = 0.4, B = 0.1 and T_{bar} = 2/3.

For the minimum speed, which corresponds to T_{bar} = 1, we notice a homogeneity in the fluctuations throughout the simulation. As the speed increases (with T_{bar} decreasing from 2/3 to 1/3), the number of disturbances increases, resulting in a less uniform Nusselt number.

Figure 10 presents the effect of the direction of movement of the bar on the average Nusselt number for Ra = 10^5, B = 0, U_{bar} = 0.4, and T_{bar} = 2/3 over a dimensionless time interval between 0 and 2. We compare the values of the Nusselt number in two cases: horizontal and vertical movements, both passing through the center of the cavity.

From the figure, we can observe a periodic behavior that repeats every Δt = 0.7. This interval corresponds to the movement of one cycle. We also notice that the horizontal movement records lower Nusselt number values compared to the vertical displacement. The peak of fluctuations is minimal when the bar is near the hot and cold walls. This can be explained by the bar generating and blocking the movement of the fluid particles in the upward and downward directions. Conversely, the peak fluctuations increase when the bar is near the center of the cavity.

4.2 | Rayleigh Number Effect

Next, we examine the effect of buoyancy force, represented by the Rayleigh number, on the distribution of isotherms, streamlines, and the development of the Nusselt number (see Figures 11, 12 and 13).

Figure 11 depicts the effect of varying the Rayleigh number from 10^4 to 10^7 on the Nusselt number for U_{bar} = 0.4, B = 0.1, and T_{bar} = 2/3. For low Rayleigh numbers, the average Nusselt number, which represents the ratio of heat transfer by convection to heat transfer by conduction, is low. This indicates that convection is less pronounced, and the periodic movement of the bar has a limited impact on local convection, leading to a slight improvement in the Nusselt number.

The increase of Ra from 10^6 to 10^7 reflects the transition from conduction-dominated to convection-dominated regimes. Higher buoyancy forces intensify circulation, generating secondary vortices and sharper temperature gradients. The moving bar further amplifies this effect by disturbing the main cells and creating additional localized convection structures, which explains the pronounced growth in the Nusselt number, where for one order of magnitude rise of Rayleigh number, the Nusselt number increases by 205% (Ra = 10^5), 195% (Ra = 10^6), and 179% (Ra = 10^7). The presence of the bar further enhances this effect, as it introduces additional disturbances that intensify convection. The additional convection cells created around the bar contribute to an overall increase in heat transfer efficiency.

Figure 12 reveals the effect of varying the Rayleigh number from 10^4 to 10^7 on the fluid circulation within the cavity for U_{bar} = 0.4, B = 0.1, and T_{bar} = 2/3. At low Rayleigh numbers, the streamlines are simple and feature symmetrical convection cells. The circulation cells are wide, and there are no eddies present in the cavity, which is due to the relatively weak air flow speeds. The negative sign of the streamlines denotes the clockwise circulation. The vertical periodic movement of the bar introduces a disturbance in the convection cells. Although the circulation remains symmetrical, the size and shape of the cells can vary depending on the bar's position.

As the Rayleigh number increases, the streamlines become more complex. Secondary vortices form in the cavity corners, and the fluid circulation speeds increase significantly, resulting in smaller and more intense circulation cells. The presence of the bar further accentuates the complexity of the flow, with additional convection cells appearing around and near the bar. The configuration and number of these cells change depending on the position of the bar.

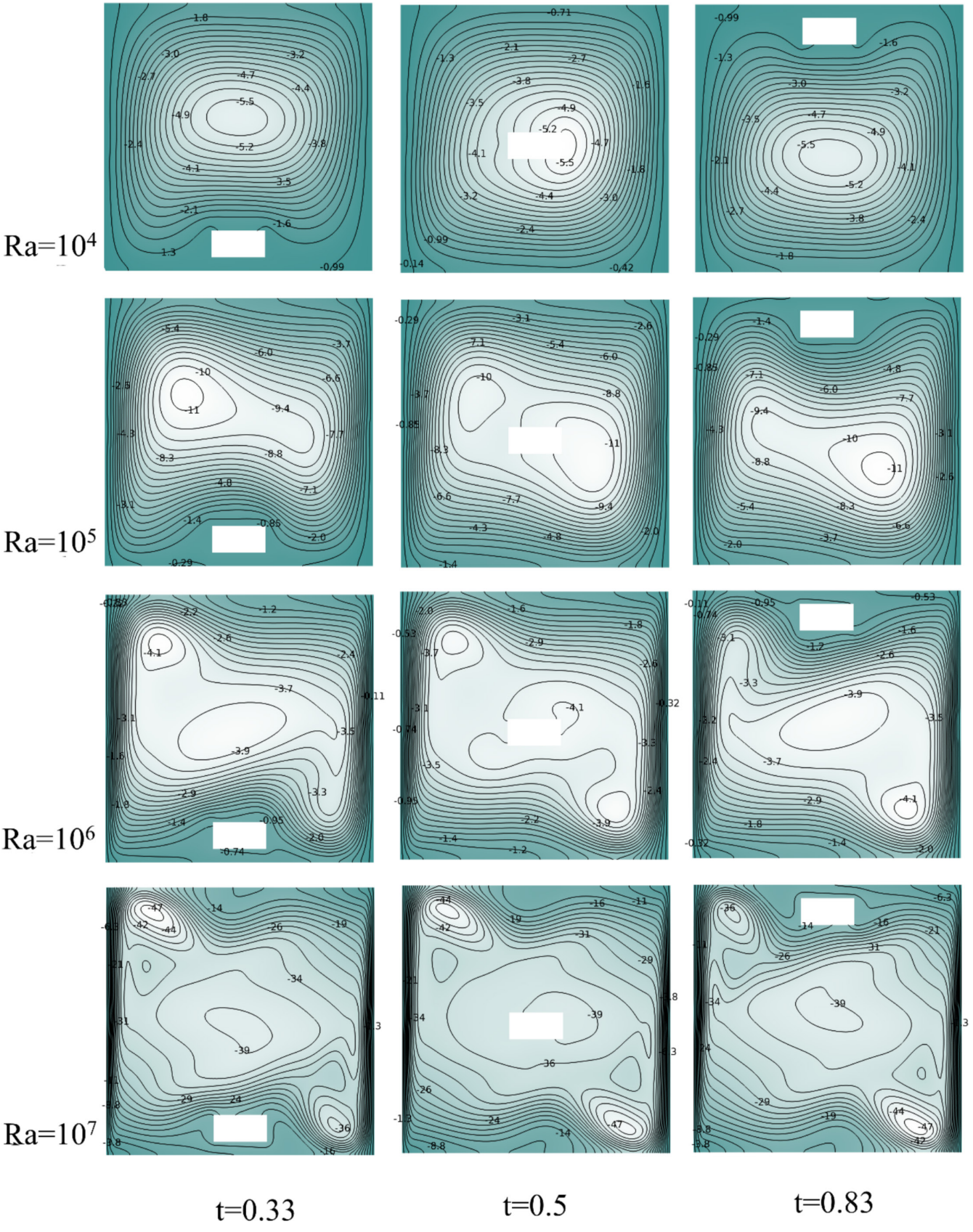

FIGURE 12 | The influence of the Rayleigh number on streamlines over time dimensionless at $U_{bar}=0.4$, $B=0.1$, and $T_{bar}=2/3$.

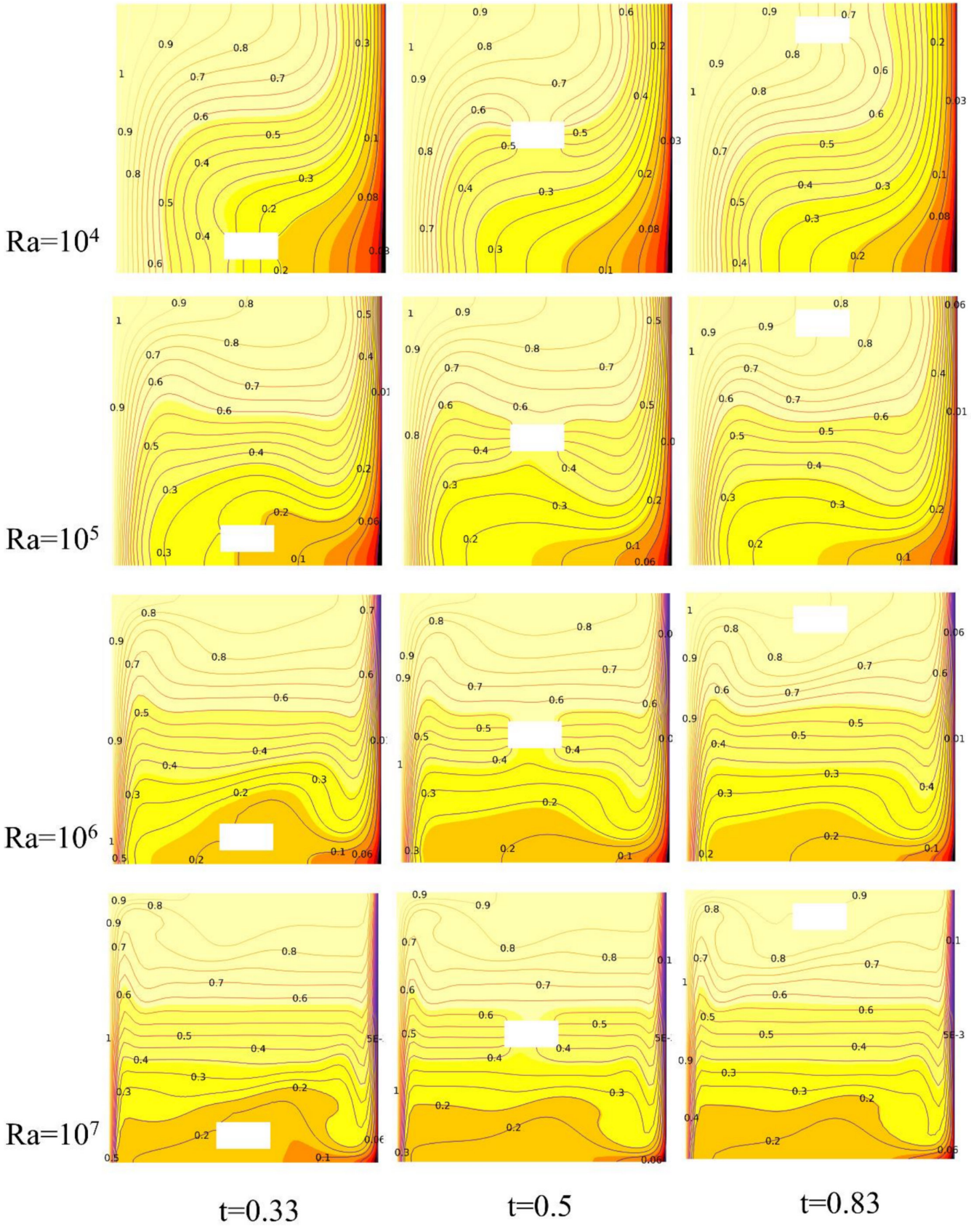

FIGURE 13 | The influence of the Rayleigh number on isotherms over time dimensionless at $U_{bar}=0.4$, $B=0.1$, $T_{bar}=2/3$.

Figure 13 displays the effect of varying the Rayleigh number from 1E4 to 10^7 on the circulation of fluid within the cavity for $U_{bar}=0.4$, $B=0.1$, and $T_{bar}=2/3$. At low Rayleigh numbers, the isotherms are relatively horizontal and parallel, indicating stable thermal diffusion. The temperature gradients are weak and uniform throughout the cavity. The presence of the bar introduces a thermal disturbance, resulting in slightly curved isotherms around the bar. Despite this, the temperature distribution remains mainly uniform, with only a slight increase in temperature gradients near the bar.

As the Rayleigh number increases, the isotherms become more curved and irregular, indicating more intense thermal convection. The temperature gradients become stronger, particularly near the hot and cold walls. The bar further deforms the isotherms, creating more pronounced temperature gradients around it. Consequently, the temperature distribution becomes more complex, with significant local variations due to the increased convection.

4.3 | Bar Geometry Effect

Figure 14 portrays the effect of varying the width of the bar B (0.05, 0.1, 0.15, and 0.2) on the distribution of isotherms within the cavity for $U_{bar}=0.4$, Ra = 1E5, and $T_{bar}=2/3$. From the figure, we can observe the following:

- **Thin bar ($B=0.05$)**: The isotherms are only slightly disturbed, showing moderate curvature around the bar. The periodic movement results in minor oscillations in the thermal distribution. The thermal fluctuations are weak but present, and the isotherms exhibit relatively small temperature gradients.
- **Wider bars ($B=0.1$, 0.15, and 0.2)**: Increasing the bar width restricts the available flow channels, which hinders fluid circulation and reduces the efficiency of convective mixing. Although wider bars intensify local gradients near their surfaces, the global heat transfer decreases because the obstruction limits the development of strong convection cells. The fluctuations in thermal distribution become more pronounced, leading to dynamic heat transfer and intense mixing.

Figure 15 illustrates the effect of varying the width of the bar B (0.05, 0.1, 0.15, and 0.2) on the circulation of fluid within the cavity for $U_{bar}=0.4$, Ra = 1E5, $T_{bar}=2/3$. From the figure, we observe the following:

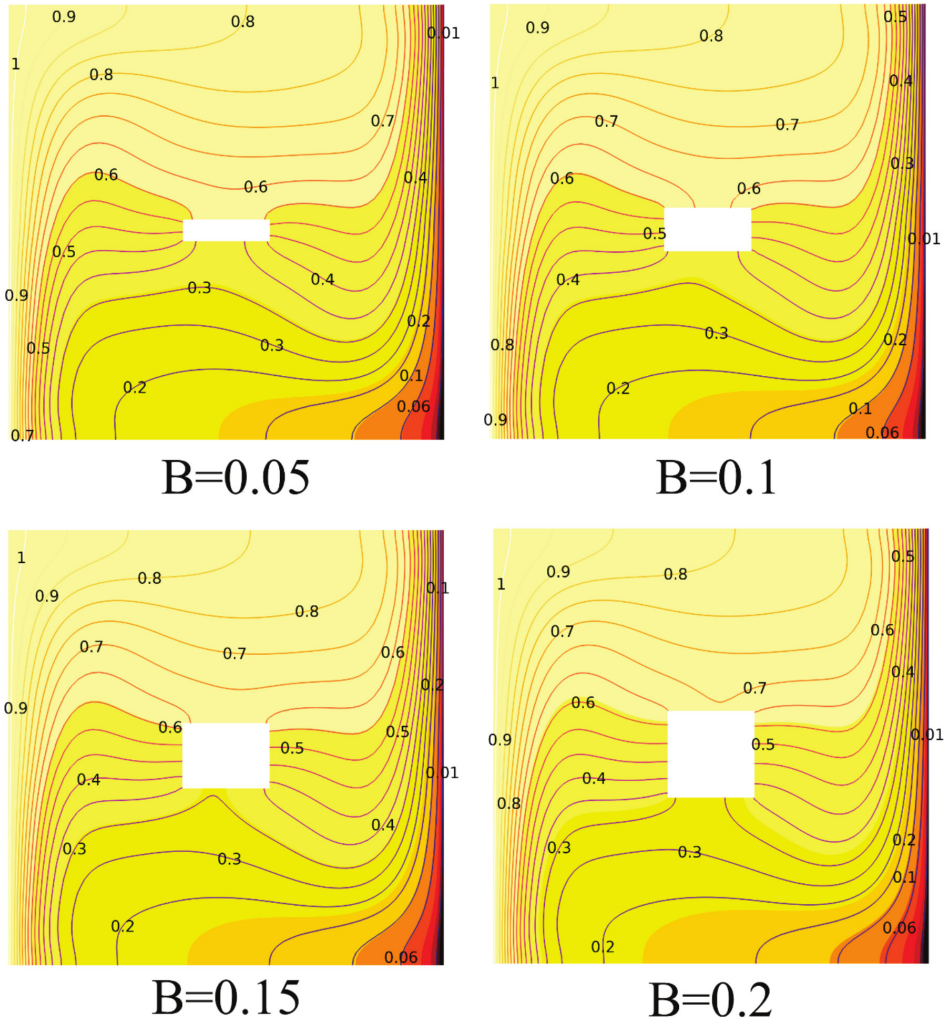

FIGURE 14 | The influence of the obstacle width B on isotherms over time dimensionless at $U_{bar}=0.4$, Ra = 10^5, $T_{bar}=2/3$.

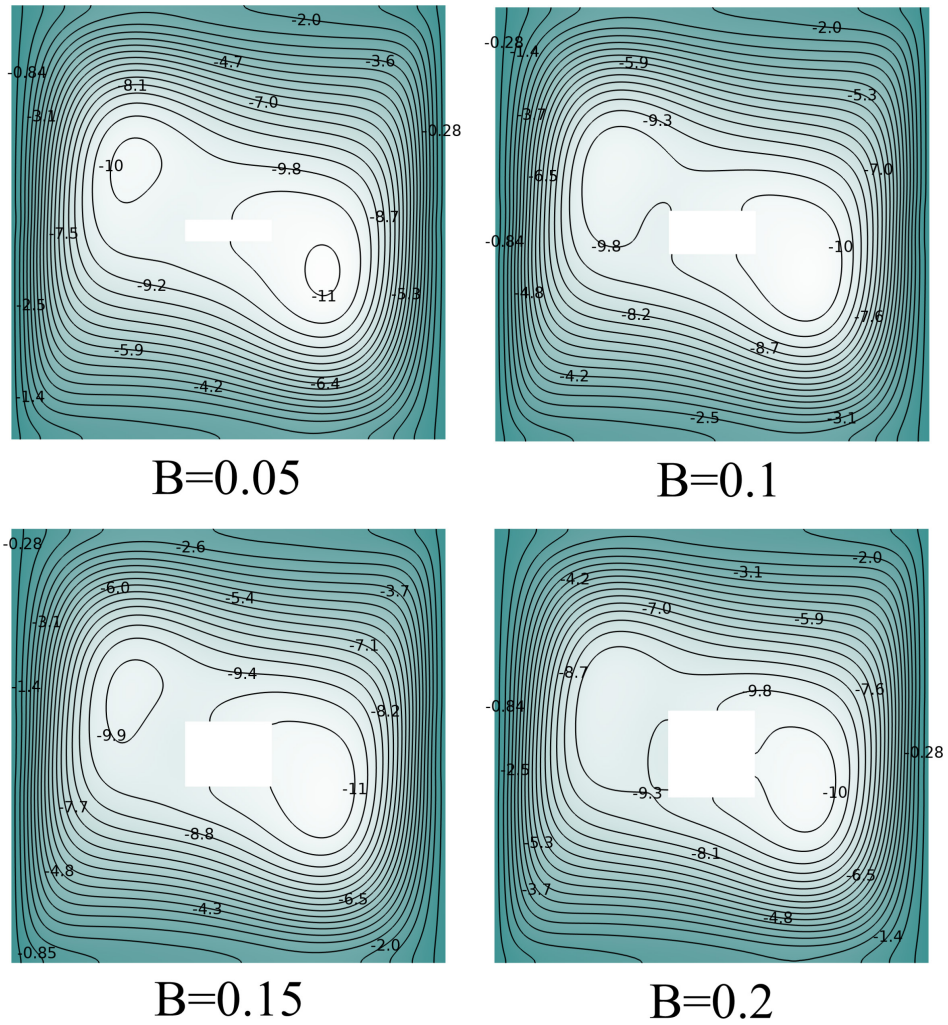

FIGURE 15 | The influence of the obstacle width B on streamlines over time dimensionless at $U_{bar} = 0.4$, $Ra = 10^6$, $T_{bar} = 2/3$.

- **Narrow bar ($B = 0.05$)**: The fluid disturbance is minimal, forming small convection cells around the bar. The vertical periodic movement introduces slight oscillatory dynamics.
- **Increasing bar width ($B = 0.1$, 0.15, and 0.2)**: As the width of the bar increases, the disruption to the streamlines becomes more pronounced. A wider bar divides the cavity into two large convection zones, with significant oscillations in the streamlines induced by the vertical movement. The periodic fluctuations become more pronounced, leading to a highly dynamic flow with constant changes in the convection cells.

Figure 16 illustrates the effect of varying the width of the bar B (0.05, 0.1, 0.15, and 0.2) on the development of the Nusselt number for $Ra = 10^5$, $U_{bar} = 0.3$, and $T_{bar} = 2/3$. From the graphical results, we can observe that for $t < 0.15$, the curves are similar, indicating that the width B has a minimal effect. Beyond this time, as the bar moves, the curves exhibit fluctuations with varying amplitudes. The most stable curve corresponds to the narrow bar, which denotes maximum Nusselt number, while the curve for the wider bar (e.g., $B = 0.2$) shows the most significant fluctuations. This variation is due to the different positions of the bar. When the bar is centrally located within the central convection cell, convection is at its maximum. Conversely, when the bar is positioned at the top or bottom, it generates natural fluid circulation, with horizontal

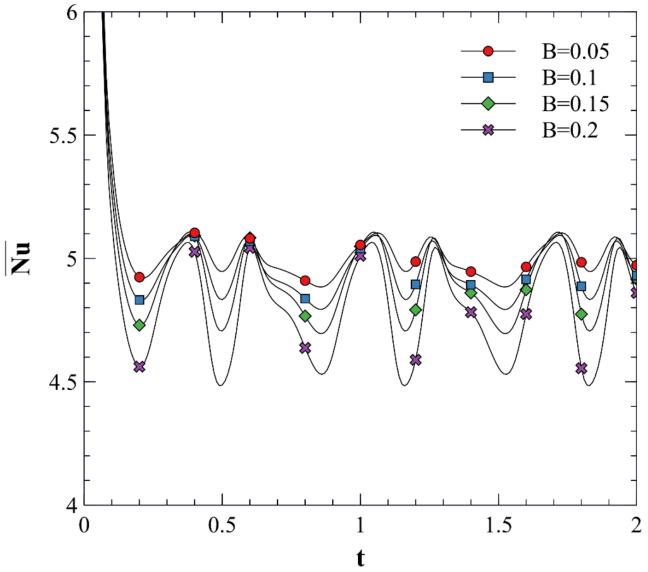

FIGURE 16 | The influence of the width of the bar on $\overline{Nu}$ over time dimensionless at $Ra = 10^5$, $U_{bar} = 0.3$, and $T_{bar} = 2/3$.

displacement constrained by the upper and lower walls, leading to less efficient convection. As the width of the bar increases, it obstructs air circulation more significantly, negatively impacting convection and heat transfer. If we consider $B = 0.05$ as a reference, we record a transfer reduction equal to 2%, 4%, and 6% which corresponds to $B = 0.1$, $B = 0.15$, and $B = 0.2$.

Figure 17 illustrates the effect of the number of bars ($N = 1, 2, 3$) on the distribution of isotherms (A) and streamlines (B) at $\mathrm{Ra} = 10^5$, $U_{\mathrm{bar}} = 0.3$ and $T_{\mathrm{bar}} = 2/3$, A = 0.2, B = 0.05.

From the figure, we can observe the following:

- **One bar**: The isotherms are perturbed around the single bar, with periodic thermal variations creating improved thermal mixing. The presence of the bar introduces oscillations in the temperature distribution, enhancing convective heat transfer.
- **Two bars**: The isotherms show more complex perturbations, with distinct curves around each bar. The interaction between the two bars generates more intricate periodic thermal variations, significantly enhancing thermal mixing.

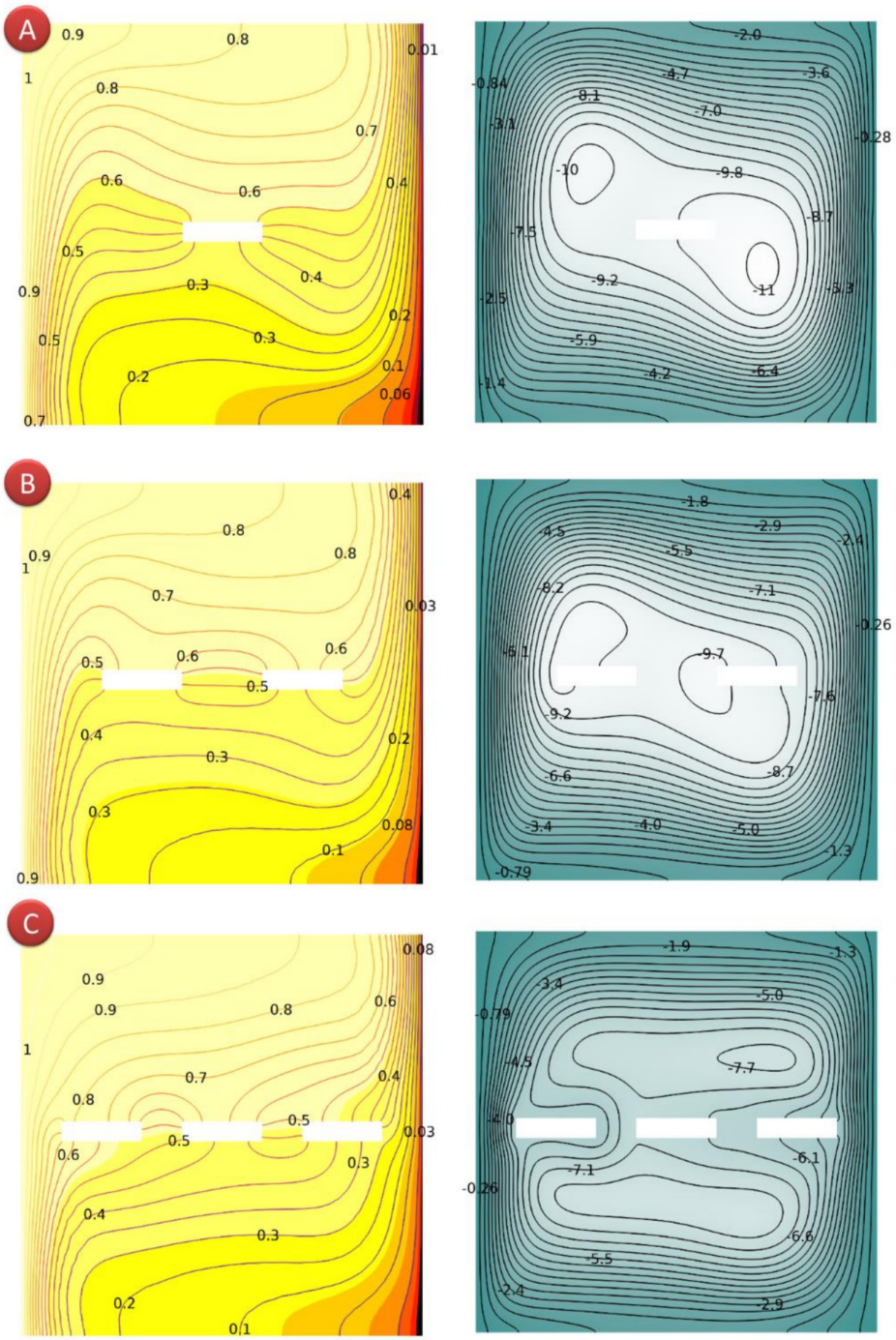

FIGURE 17 | The influence of number of bars ($N = 1, 2, 3$) on the distribution of stream lines (right) and isotherms (left) at $\mathrm{Ra} = 10^5$, $U_{\mathrm{bar}} = 0.3$, and $T_{\mathrm{bar}} = 2/3$, A = 0.2, B = 0.05.

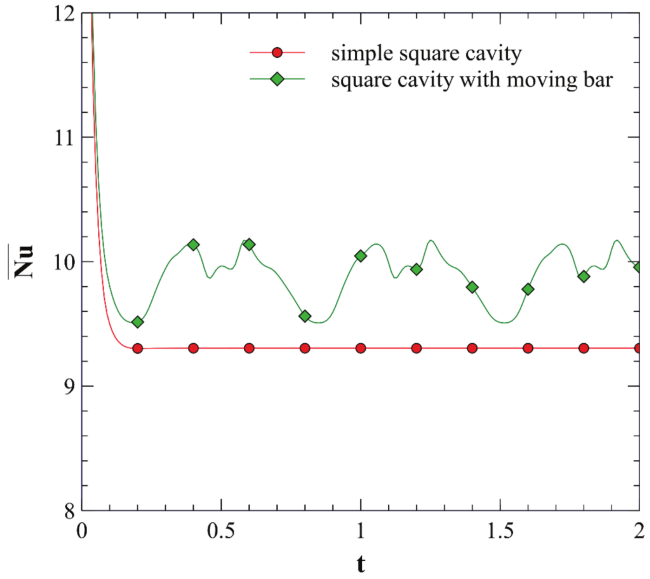

FIGURE 18 | Comparison between the averaged Nusselt for simple square cavity (without moving bar) and cavity with bar for Ra = 10^6, $U_{bar} = 0.4$, and $T_{bar} = 1$, A = 0.2, B = 0.1.

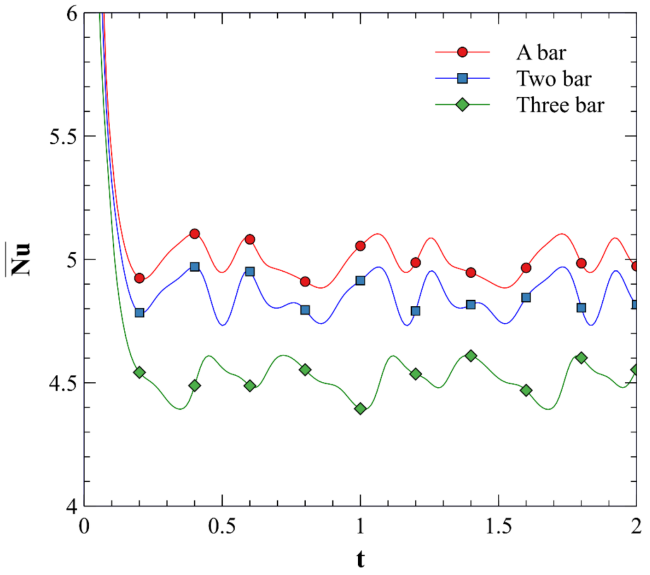

FIGURE 19 | The influence of bar number ($N = 1, 2, 3$) on the average Nusselt number at Ra = 10^6, $U_{bar} = 0.3$, and $T_{bar} = 2/3$, A = 0.2, B = 0.05.

- **Three bars**: The presence of three bars results in even more complex thermal perturbations. The isotherms exhibit pronounced curves around each bar, with the interaction among multiple bars further improving thermal mixing.

For the distribution of streamlines:

- **One bar**: The cavity is divided into two distinct convection zones by the single bar. The periodic movement of the bar induces oscillations in the convection currents, creating dynamic mixing and disturbances.
- **Two bars**: The presence of two bars leads to more complex convection zones. Convection cells form around each bar and interact with each other, creating a more intricate flow pattern.
- **Three bars**: With three bars, the convection zones become even more complex. The interactions among multiple bars result in a highly dynamic flow, with numerous convection cells interacting and overlapping.

To **examine** the role of the moving bar on the natural convection, a comparison between the pure convection case (without the bar) and the case of a single moving bar at Ra = 10^6 is performed. Graphically, Figure 18 demonstrates the virtue of the moving bar by elevating the periodic Nusselt number. The percentage enhancement in the Nusselt number can reach 7%.

Figure 19 presents the effect of varying the number of bars ($N = 1$, 2, 3) on the average Nusselt number for Ra = 10^5, $U_{bar} = 0.3$, and $T_{bar} = 2/3$, A = 0.2, B = 0.05.

From the figure, we observe the following:

- **Initial state**: In the initial state, the curves for different numbers of bars are identical and coincide, indicating that the presence of bars has a negligible effect on the average Nusselt number at this stage. After a dimensionless time $t = 0.2$, fluctuations begin to emerge due to the periodic movement of the bars.
- **Effect of increasing number of bars**: As the number of bars increases, there is a noticeable decrease in the average Nusselt number. If we consider a bar as a reference, the presence of two bars leads to a decrease of 2%, and three bars a decrease of 6%. This reduction in heat transfer efficiency can be attributed to the increased disturbance caused by the vertical movement of multiple bars. This disturbance impairs the natural circulation of the fluid within the cavity, leading to a decreased effectiveness of convection and, consequently, a lower average Nusselt number.

5 | Conclusions

The present study investigates the effect of the periodic motion of a rectangular bar on natural convection within a square cavity. The problem is addressed using the finite element method with a moving mesh to accommodate the bar's movement. The influence of various parameters was analyzed, including the direction of the bar's movement (horizontal and vertical), amplitude of displacement (U_{bar}), period of displacement (T_{bar}), width of the bar (B), and Rayleigh number (Ra), and number of bars (N). The key conclusions are as follows:

- **Effect of vertical bar movement**: The vertical movement of the bar significantly impacts the average Nusselt number. An increase in the amplitude of displacement (U_{bar}) leads to a decrease in the Nusselt number, while an increase in the period of displacement (T_{bar}) promotes thermal homogeneity. For optimal heat transfer, it is recommended to use $T_{bar} = 1$ and U_{bar} with vertical displacement.
- **Rayleigh number and bar movement**: The coupling between the Rayleigh number and the periodic movement of the bar affects the distribution of streamlines and isotherms.

Higher Rayleigh numbers result in more complex secondary convection cells around the bar. The bar's movement introduces additional convective flow, which improves the Nusselt number.

- **Geometry of the bar**: The bar's geometry plays a crucial role in heat transfer. A narrow bar ($B = 0.05$) enhances heat transfer and creates minimal obstruction to horizontal air movement. The impact on streamlines and isotherms is less pronounced with a narrow bar. Conversely, increasing the bar's width negatively affects heat transfer by obstructing natural air movement. Therefore, $B = 0.05$ is ideal for optimal heat transfer.
- **Number of bars**: Increasing the number of bars has a detrimental effect on the Nusselt number and heat transfer efficiency. Using a single bar is sufficient for effective heat transfer.

These findings highlight potential applications in thermal engineering systems where efficient natural convection is essential. In particular, the results may contribute to the design of advanced cooling technologies for electronic devices, compact heat exchangers, and energy storage systems, where dynamic obstacles could be exploited to optimize heat transfer performance.

Nomenclature

Latin

A, B	dimensionless length and width of the bar
g_y	gravitational acceleration
h	the convective heat transfer coefficient
k^{air}	thermal conductivity
L	cavity length
Nu	average Nusselt number
P	dimensionless pressure
Pr	Prandtl number
Ra	Rayleigh number
t	dimensionless time
T	dimensionless temperature
T_{bar}	dimensionless period of bar displacement
u°, v° and u_{air}, v_{air}	dimensional and dimensionless velocity components
U_{bar}	dimensionless amplitude of bar displacement
X,Y	the dimensionless Cartesian coordinates
X_{bar}	dimensionless displacement of the bar

Greek symbols

α_{air}	thermal diffusivity
β	the coefficient of thermal expansion
μ	dynamic viscosity
ρ_{air}	density
υ_{air}	kinematic viscosity
Ψ	non-dimensional stream function

Subscript

c, h	cold, hot

Acknowledgments

The first author would like to thank the officials of the Directorate General for Scientific Research and Technological Development (DGRSDT) for having included this journal so that Algerian researchers can contribute to the development of their research in this field.

Conflicts of Interest

The authors declare no conflicts of interest.

Data Availability Statement

The data that support the findings of this study are available from the corresponding author upon reasonable request.

References

1. N. Tarek, and M. Ismael, "The Role of Periodic Mixing on Thermal Energy Extraction From an L-Shaped Heater Covered by Porous Layer," *Heat Transfer* 54, no. 3 (2025): 1851–1864, https://doi.org/10.1002/htj.23265.

2. A. Raji, M. Hasnaoui, M. Naïmi, K. Slimani, and M. T. Ouazzani, "Effect of the Subdivision of an Obstacle on the Natural Convection Heat Transfer in a Square Cavity," *Computers & Fluids* 68 (2012): 1–15, https://doi.org/10.1016/j.compfluid.2012.07.014.

3. Z. Boulahia, "Numerical Investigation of Mixed Convection Heat Transfer of Nanofluid in a Lid Driven Square Cavity with Three Triangular Heating Blocks," *International Journal of Computer Applications* 143, no. June (2016): 37–45, https://doi.org/10.5120/ijca2016910227.

4. M. Umme, M. Maya, N. Alam, and A. R. Ali, "Influence of Magnetic Field on MHD Mixed Convection in Lid-Driven Cavity With Heated Wavy Bottom Surface," *Scientific Reports* 13, no. 0123456789, (2023): 1–19, https://doi.org/10.1038/s41598-023-45707-x.

5. A. R. Rahmati, and A. A. Tahery, "Numerical Study of Nanofluid Natural Convection in a Square Cavity With a Hot Obstacle Using Lattice Boltzmann Method," *Alexandria Engineering Journal* 57, no. 3 (2018): 1271–1286, https://doi.org/10.1016/j.aej.2017.03.030.

6. W. Aich, I. Hilali-Jaghdam, A. Alshahrani, C. Maatki, B. M. Alshammari, and L. Kolsi, "Control of Three-Dimensional Natural Convection of Graphene–Water Nanofluids Using Symmetrical Tree-Shaped Obstacle and External Magnetic Field," *Symmetry* 16, no. 6 (2024): 692, https://doi.org/10.3390/sym16060692.

7. A. Mirzaei, P. Jalili, M. Dehghan, and B. Jalili, "Convection Heat Transfer of MHD Fluid Flow in the Circular Cavity With Various Obstacles: Finite Element Approach," *International Journal of Thermofluids* 20, no. November (2023): 100522, https://doi.org/10.1016/j.ijft.2023.100522.

8. M. I. Elkhazen, D. Akrour, W. Hassen, et al., "Effect of an Adiabatic Obstacle on the Symmetry of the Temperature, Flow, and Electric Charge Fields during Electrohydrodynamic Natural Convection," *Symmetry* 16, no. 6 (2024): 761, https://doi.org/10.3390/sym16060761.

9. H. A. Nabwey, A. M. Rashad, P. B. Anki, S. Jakeer, M. A. Mansour, and T. Salah, "Radiative Effects on Unsteady MHD Natural Convection Flow in an Inclined Wavy Porous Cavity Using Hybrid Nanofluid Containing a Square Obstacle," *Alexandria Engineering Journal* 65 (2023): 921–937, https://doi.org/10.1016/j.aej.2022.10.004.

10. G. Yan, A. Rahmani, and M. Zarringhalam, "Natural Convection of Rectangular Cavity Enhanced by Obstacle and Fin to Simulate Phase Change Material Melting Process Using Lattice Boltzmann Method," *Alexandria Engineering Journal* 81, no. September (2023): 319–336, https://doi.org/10.1016/j.aej.2023.09.035.

11. Rashid, U., Lu, D., and Iqbal, Q., "Case Studies in Thermal Engineering Nanoparticles Impacts on Natural Convection Nanofluid Flow and Heat Transfer Inside a Square Cavity With Fixed a Circular Obstacle," *Case Studies in Thermal Engineering* 44, no. February (2023): 102829, https://doi.org/10.1016/j.csite.2023.102829.

12. F. Selimefendigil, "Natural Convection and Entropy Generation of Nanofluid Filled Cavity Having Different Shaped Obstacles Under the Influence of Magnetic Field and Internal Heat Generation," *Journal of the Taiwan Institute of Chemical Engineers* 56 (2015): 42–56, https://doi.org/10.1016/j.jtice.2015.04.018.

13. S. Ahmad, B. M. Cham, D. Liu, S. U. Islam, M. A. Hussien, and H. Waqas, "Numerical Analysis of Heat and Mass Transfer of MHD

Natural Convection Flow in a Cavity With Effects of Source and Sink," *Case Studies in Thermal Engineering* 53, no. September 2023 (2024): 103926, https://doi.org/10.1016/j.csite.2023.103926.

14. A. H. Majeed, R. Mahmood, and D. Liu, "Finite Element Simulations of Double Diffusion in a Staggered Cavity Filled With a Power-Law Fluid," *Physics of Fluids* 36, no. 3 (2024): 033101, https://doi.org/10.1063/5.0189237.

15. S. Ahmad, Y. u. U. B. Turabi, D. Liu, H. Waqas, and S. Munir, "Numerical Simulation of Magnetohydrodynamics Double-Diffusive Natural Convection in a Cavity With Non-Uniform Heated Walls," *Applied Thermal Engineering* 253 (2024): 123778, https://doi.org/10.1016/j.applthermaleng.2024.123778.

16. S.-L. Sun, D. Liu, Y.-Z. Wang, Y.-L. Qi, and H.-B. Kim, "Convective Heat Transfer and Entropy Generation Evaluation in the Taylor–Couette Flow Under the Magnetic Field," *International Journal of Mechanical Sciences* 252 (2023): 108373, https://doi.org/10.1016/j.ijmecsci.2023.108373.

17. A. T. Franco, P. R. M. Santos, A. Lugarini, et al., "The Effects of Discrete Conductive Blocks on the Natural Convection in Side-Heated Open Cavities," *Applied Thermal Engineering* 219 (2023): 119613, https://doi.org/10.1016/j.applthermaleng.2022.119613.

18. N. Tarek, B. Elhadj, G. Mohammad, H. Mohammed, and A. Khadidja, "Fluid-Structure Interaction Study of an Oscillating Heat Source Effect on the Natural Convection Flow," *Heat Transfer* 53 (2024): 2369–2390, https://doi.org/10.1002/htj.23037.

19. J. Sarrate, A. Huerta, and J. Donea, "Arbitrary Lagrangian–Eulerian Formulation for Fluid–Rigid Body Interaction," *Computer Methods in Applied Mechanics and Engineering* 190, no. 24–25 (2001): 3171–3188, https://doi.org/10.1016/S0045-7825(00)00387-X.

20. A. Joda, Z. Jin, J. Summers, and S. Korossis, "Comparison of a Fixed-Grid and Arbitrary Lagrangian–Eulerian Methods on Modelling Fluid–Structure Interaction of the Aortic Valve," *Proceedings of the Institution of Mechanical Engineers, Part H, Journal of Engineering in Medicine* 233, no. 5 (2019): 544–553, https://doi.org/10.1177/0954411919837568.

21. N. Tarek, B. Elhadj, H. Mohammed, A. Khadidja, "Numerical Simulation of Fluid-Structure Interaction in Undulated Cavity Numerical Simulation of Fluid-Structure Interaction in Undulated Cavity," *International Journal of Heat and Technology* 41, No. 5 (2023): 1205–1216, https://doi.org/10.18280/ijht.410511.

22. T. Tang, "Moving Mesh Methods for Computational Fluid Dynamics," *Recent Advances in Adaptive Computation* 383 (2005): 141–173, https://doi.org/10.1090/conm/383/07162.

23. W. Huang, Y. Ren, and R. D. Russell, "Moving Mesh Methods Based on Moving Mesh Partial Differential Equations 1 Introduction," *Journal of Numerical Analysis* 31, no. 3 (1995): 709–730, https://www.jstor.org/stable/2158026.

24. B. S. Kim, D. S. Lee, M. Y. Ha, and H. S. Yoon, "A Numerical Study of Natural Convection in a Square Enclosure With a Circular Cylinder at Different Vertical Locations," *International journal of heat and mass transfer* 51, no. 7–8 (2008): 1888–1906, https://doi.org/10.1016/j.ijheatmasstransfer.2007.06.033.

25. B. Calcagni, F. Marsili, and M. Paroncini, "Natural Convective Heat Transfer in Square Enclosures Heated From Below," *Applied Thermal Engineering* 25, no. 16 (2005): 2522–2531, https://doi.org/10.1016/j.applthermaleng.2004.11.032.

26. G. De Vahl Davis, "Natural Convection of Air in a Square Cavity: A Bench Mark Numerical Solution," *International Journal for Numerical Methods in Fluids* 3, no. 3 (1983): 249–264, https://doi.org/10.1002/fld.1650030305.

27. A. Raji, M. Hasnaoui, and M. Firdaouss, "Natural Convection Heat Transfer Enhancement in a Square Cavity Periodically Cooled From Above," 2015 (2013), https://doi.org/10.1080/10407782.2013.733248.